Anyon braiding and telegraph noise in a graphene interferometer

Thomas Werkmeister,[1,†] James R. Ehrets,[2,†] Marie E. Wesson,[1] Danial H. Najafabadi,[3] Kenji Watanabe,[4] Takashi Taniguchi,[5] Bertrand I. Halperin,[2] Amir Yacoby,[1,2] Philip Kim[1,2,*]

[1] *John A. Paulson School of Engineering and Applied Sciences, Harvard University, Cambridge, MA 02138, USA*
[2] *Department of Physics, Harvard University, Cambridge, MA 02138, USA*
[3] *Center for Nanoscale Systems, Harvard University, Cambridge, MA 02138, USA*
[4] *Research Center for Electronic and Optical Materials, National Institute for Materials Science, 1-1 Namiki, Tsukuba 305-0044, Japan*
[5] *Research Center for Materials Nanoarchitectonics, National Institute for Materials Science, 1-1 Namiki, Tsukuba 305-0044, Japan*

(Dated: May 26, 2026)

The search for anyons, quasiparticles with fractional charge and exotic exchange statistics, has inspired decades of condensed matter research. Quantum Hall interferometers enable direct observation of the anyon braiding phase via discrete interference phase jumps when the number of encircled localized quasiparticles changes. Here, we observe this braiding phase in both the $\nu = 1/3$ and 4/3 fractional quantum Hall states by probing three-state random telegraph noise (RTN) in real-time. We find that the observed RTN stems from anyon quasiparticle number n fluctuations and reconstruct three Aharonov-Bohm oscillation signals phase shifted by $2\pi/3$, corresponding to the three possible interference branches from braiding around n (mod 3) anyons. Our methods can be readily extended to interference of non-abelian anyons.

The fractional quantum Hall (FQH) effects, where electrons are confined to two spatial dimensions and exposed to large magnetic fields, have long been predicted to host emergent fractionally charged excitations that obey neither fermionic nor bosonic exchange statistics [1–5]. These quasiparticles fall into two classes, abelian and non-abelian anyons, associated with FQH states at different filling factors ν. For abelian anyons, exchanging two quasiparticles (i.e. braiding) results in the many-body wavefunction acquiring a complex phase, as demonstrated by anyon collision and interferometry experiments [6, 7]. For non-abelian anyons, the wavefunction evolves by a unitary transformation, enabling fault-tolerant topological quantum computation that has yet to be experimentally realized [8–12].

FQH Fabry-Pérot (FP) interferometers enable direct measurements of the anyon braiding phase [13, 14]. By partially backscattering current at two quantum point contact (QPC) constrictions, the conductance through the FP cavity modulates with the phase accumulated by edge-traveling quantum Hall (QH) quasiparticles [5, 15]. When the number of localized cavity quasiparticles encircled by the interfering edge changes, the resulting phase shift in the interference signal is equivalent to twice the fundamental exchange phase (modulo 2π) [7, 16]. However, because the observed discrete phase jumps represent charging events in the cavity, resultant Coulomb coupling between the bulk and edge must be accounted for when extracting the anyon braiding phase from a small number of phase jump events [17]. Consequently, mitigating Coulomb coupling while maintaining electrostatic tunability has been a major challenge in semiconductor-based interferometers [7, 18].

Graphene-based interferometers offer several advantages for realizing anyon braiding, both for the abelian and non-abelian cases. First, both QPCs [19, 20] and interferometers [21–26] exhibit robust electrostatic tunability for integer QH states. Second, graphite gates reduce Coulomb coupling to reveal Aharonov-Bohm (AB) oscillations [22], which previously required complex quantum well structures in GaAs [7, 18]. Simultaneously, these atomically-flat gates enhance FQH states by screening out charge disorder [27, 28] while allowing precise control of QPC transmission [22, 29, 30] and FP cavity filling factor [25]. Encouragingly, bilayer graphene has displayed a multitude of even-denominator FQH states which may host non-abelian anyons with relatively large energy gaps [31–35]. Here we report direct observation of abelian anyon braiding using high-visibility Aharonov-Bohm interference and anyon fluctuations in single atomic layer graphene.

Constructing a graphene fractional quantum Hall interferometer

We construct our device by performing previously described nanolithography steps [22, 25] on a heterostructure consisting of monolayer graphene encapsulated with insulating hexagonal boron nitride [36] and conducting graphite layers. By gating with separated top graphite regions, we define the interferometer cavity and construct two QPCs that introduce backscattering between the opposite chirality QH edge channels (Fig. 1A). The quality of the graphene is maintained in part thanks to the encapsulating graphite gates, as evident by well-developed

† These authors contributed equally to this work
* Corresponding author. Email: pkim@physics.harvard.edu

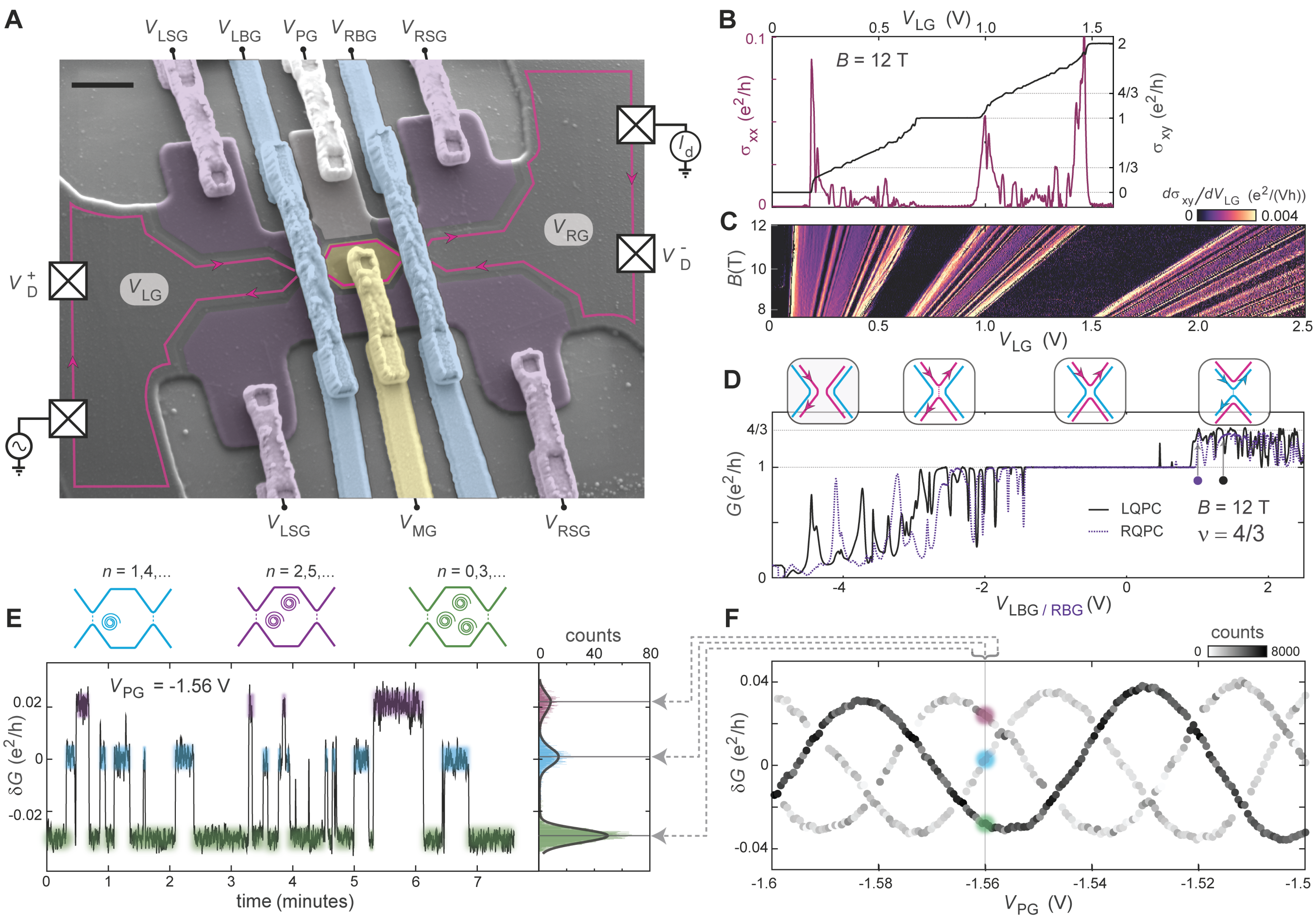

FIG. 1. **Graphene FQH interferometer telegraph noise.** (**A**) False-color scanning electron microscope image of a representative device depicting an interference measurement with a single edge channel. Scale bar: 1 μm. We measure the conductance $G = I_d/(V_D^+ - V_D^-)$ where I_d is the measured drain current and $V_D^\pm$ are the measured voltages at the indicated locations. The top graphite gate is etched into 8 separately tunable regions controlled by voltages V_{LG}, V_{LSG}, V_{PG}, V_{MG}, V_{RSG}, and V_{RG}. Additionally, voltages $V_{LBG/RBG}$ applied to suspended bridges above the two QPCs independently set their transmissions. See Fig. S1 for more details. (**B**) Hall conductivity σ_{xy} and longitudinal conductivity σ_{xx} measured with contacts in the left reservoir of the device highlighting the robust plateaus at $\nu = 0$, 1/3, 1, and 4/3, the quantum Hall states that we study. (**C**) Derivative of σ_{xy} showing the expected magnetic field dependence of the well-developed quantum Hall states. (**D**) Conductance G across the left/right QPC tuned by $V_{LBG/RBG}$ with the right/left QPC deactivated and the bulk in $\nu = 4/3$. See Fig. S2 for details. Inset: schematics of the edge channel configuration and tunneling at a QPC. As $V_{LBG/RBG}$ increases, the constriction opens and transmits the outer integer edge (pink) first and eventually transmits the inner fractional edge (blue). (**E**) Three-state RTN in the conductance G when the fractional edge of $\nu = 4/3$ is weakly backscattering, corresponding to the tuning $V_{LBG} = 1.37$ V and $V_{RBG} = 1.01$ V, marked by the black and purple dots, respectively in (D), which are chosen to set $G \approx 1.28\, e^2/h$ or roughly 15% backscattering at each QPC. Top inset: cartoons of the three possible interference branches from braiding around n (mod 3) anyons, corresponding to the three conductance levels. Right inset: histogram of the conductance over time with 1000 bins. (**F**) Extracted sinusoidal oscillations from histograms over approximately 8 minutes for each V_{PG} voltage. Each data point shows the central conductance value of a gaussian fit to a histogram peak, shaded by the total counts summed under the gaussian. See Fig. S3 for similar data in $\nu = 1/3$.

FQH states (Fig. 1B and C) at $T = 20$ mK. Unlike previous FQH interferometers in GaAs, we can tune the electron density in-situ in graphene to access many FQH states while holding the magnetic field fixed. Here we set magnetic field $B = 12$ T (unless noted otherwise) and change density to tune between filling factors $\nu = 4/3$, $\nu = 1$, and $\nu = 1/3$, enabling a direct comparison of interference between each state.

We begin by tuning the device such that the interferometer cavity and adjoining contact regions are set to $\nu = 4/3$ by applying appropriate voltages V_{MG}, V_{LG}, and V_{RG}. The cavity boundary is defined by setting the plunger gate (V_{PG}) and QPC split-gate regions ($V_{LSG/RSG}$) to lie within $\nu = 0$. Two additional metallic bridge gates over the QPCs ($V_{LBG/RBG}$) allow for independent control of QPC transmissions while keeping all other gates fixed. The conductance across each QPC evolves from near 0 to a plateau at e^2/h, and finally to near $(4/3)e^2/h$ with increasing $V_{LBG/RBG}$, where e is the electron charge and h is Planck's constant (Fig. 1D). The resonances in the conductance in these scans indicate a relatively soft confining potential at this QPC tuning [29, 37]. It is then straightforward to tune each QPC to weakly backscatter the fractional edge channel of $\nu = 4/3$ by setting $V_{LBG/RBG}$ as indicated in Fig. 1D.

Three-state anyon telegraph noise

By measuring the conductance through the interferometer with the fractional edge of $\nu = 4/3$ weakly backscattering at both QPCs, we discover sporadic switches between three discrete levels as a function of time i.e. three-state RTN (Fig. 1E). From a histogram showing how these levels are weighted over 8 minutes, we extract the average conductance and the total weight in time associated with each level. Then, we step the plunger gate V_{PG} to modify the area [18, 22, 38, 39], or equivalently the total charge [25, 40] contained in the FP cavity, and repeat the process. Plotting the resulting average conductance values shaded by their weight in time as a function of V_{PG} reveals three interwoven, phase-shifted sinusoidal oscillations (Fig. 1F).

Each sinusoid represents one of the three n (mod 3) possible phase "branches" associated with braiding the interfering edge quasiparticles around a system composed of n $e/3$ abelian anyons [41–43]. By fitting the phase shift between the sinusoids using an improved measurement style (see next section), we are able to extract the braiding phase to high precision.

Demonstrating exchange statistics with RTN is a departure from the method used in previous interferometer studies, in which discrete phase jumps in the continuously modulating AB phase $\theta_{AB}(B, V_{PG})$ were argued to represent the addition or subtraction of a quasiparticle in the interferometer bulk [7, 17, 44]. These studies rely on modulating the AB phase using magnetic field B and plunger gate V_{PG} to probe irregularly spaced phase jumps due to anyon localization. In order to extract the anyon braiding phase, however, the experimentally observed phase jumps need to be analyzed with consideration given to the electrostatic coupling between the QH edge and localized bulk states. These analyses often become complicated as the bulk-edge capacitive coupling, the position of the chemical potential relative to the bulk Landau levels, and interferometer area A can drastically impact interference behavior, such as pivoting the interference signal into the well-studied "Coulomb-dominated" regime [14, 17, 38, 45, 46]. It has also been shown that integer quantum Hall fillings can produce similar fractional phase jumps owing to the Coulomb coupling effect described above [25, 26, 47, 48].

The measurement scheme presented in our work, i.e. observing a time-dependent interference phase ϕ through the RTN signal, offers a key benefit in this regard. Here the parameters (B, V_{PG}) used to modulate the AB phase

$$\theta_{AB}(B, V_{PG}) = 2\pi \frac{e^*}{e} \frac{A(V_{PG})B}{\phi_0}$$

can be held fixed while the quasiparticle number $n(t)$ fluctuates in time. Then, the expression for the total interference phase may be simplified as

$$\phi = \theta_{AB}(B, V_{PG}) + n(B, V_{PG}, t)\ \theta_a \rightarrow \theta_{AB} + n(t)\ \theta_a \quad (1)$$

where $\theta_a = 2\pi/3$ is the braiding phase for an $e^* = e/3$ anyon around a localized counterpart (assuming that Coulomb interactions are well screened) and $\phi_0 = h/e$. Considering the 2π periodicity of ϕ, the resulting braiding phase can only be one of three values varying by $2\pi/3$, reflecting the total number of localized anyons $n(t)$ (mod 3) at a given time. The device accordingly remains static in configurable parameter space (B, V_{PG}) while observing conductance switching from real-time fluctuations $n(t)$. Therefore, as this method demonstrates the existence of all three branches associated with the exchange statistics of charge $e/3$ anyons, we construct a complete representation of the state's braiding outcomes near a fixed device configuration set by B, V_{PG}, and density (tuned via V_{MG}).

Aharonov-Bohm magnetic field dependence

Measuring how the magnetic field B changes the total interference phase is crucial in determining if the interferometer falls into the AB or Coulomb-dominated regime [5, 14]. We start for comparison with the $\nu = 1$ integer QH state. By repeatedly sweeping the plunger gate, we observe the expected single-sinusoidal oscillations devoid of phase jumps (Fig. 2A). As we change B, we observe magnetic-field dependent AB interference (Fig. 2B), where the magnetic field period ΔB_1 yields an area $\phi_0/\Delta B_1 = 0.80\ \mu\text{m}^2$, as expected for interference of electrons in $\nu = 1$. A similar measurement in $\nu = 1/3$ with varying B and V_{PG} produces an irregular 2D map because repeated plunger gate sweeps are not consistent due to the frequent RTN fluctuations (Fig. 2C). However, we observe that each plunger gate scan contains stochastic switching between 3 sinusoidal branches, again shifted by $2\pi/3$ (Fig. 2D). By superimposing 100 of these sweeps and plotting the histogram of total recorded conductance values over V_{PG}, we are able to sample enough instances of the AB oscillation signal of each branch to recreate the three interwoven sinusoids seen in the previous measurement technique discussed in Fig. 1. Figure 2E exhibits the three interwoven branches at different magnetic fields. As the magnetic field decreases (from the top to bottom panels), we observe that each branch continuously drifts towards increasing V_{PG} values, creating a negative slope of constant phase (dashed line) analogous to the integer case of Fig. 2B. For $\nu = 1/3$, the corresponding flux super-periodicity $\Delta B_{1/3}$ (the magnetic

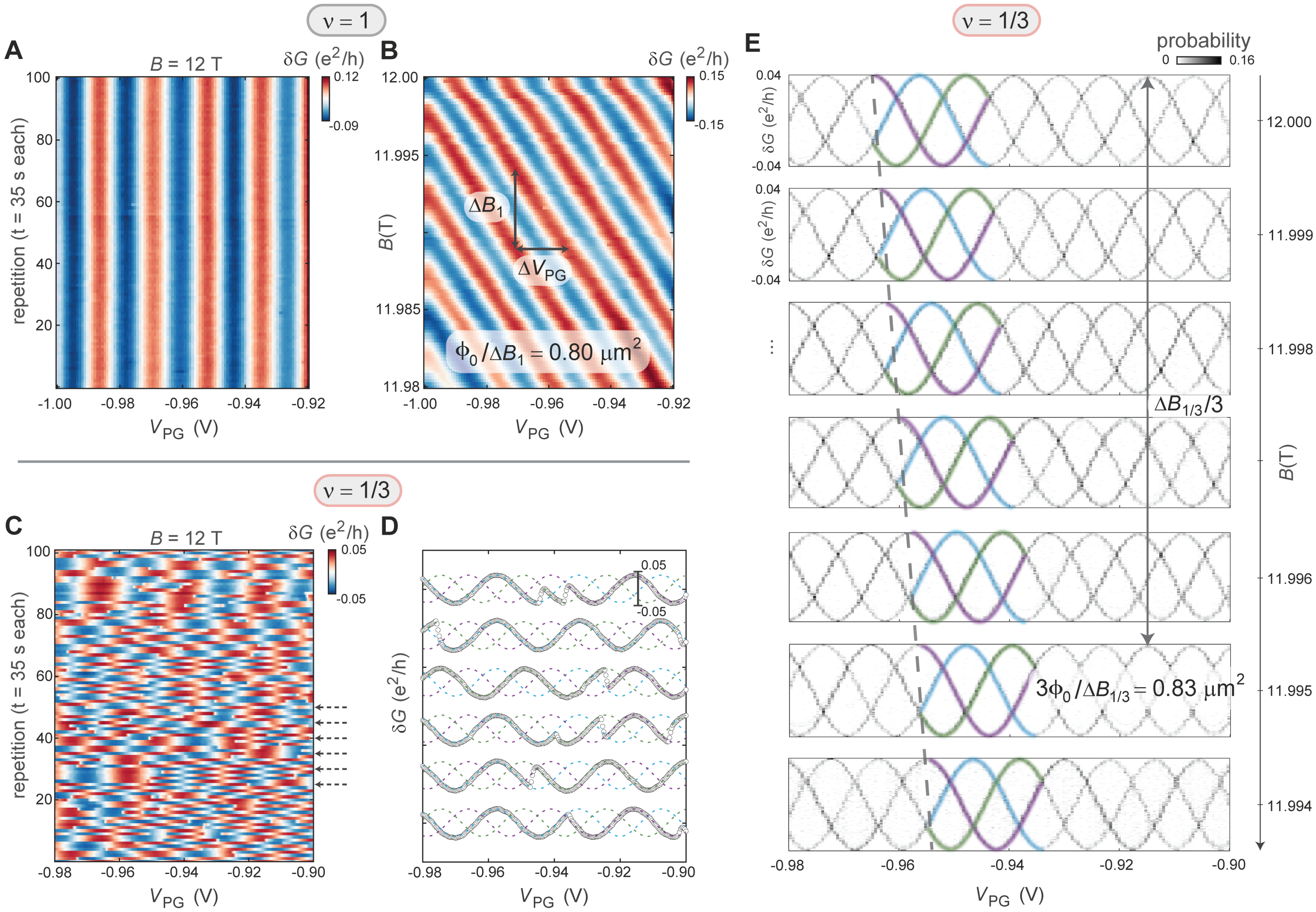

FIG. 2. **Aharonov-Bohm magnetic field trend of $\nu = 1/3$ branches.** (**A**) 100 repeated V_{PG} sweeps in $\nu = 1$, where each sweep takes 35 s, demonstrating the temporal stability of oscillations in the integer state. (**B**) Magnetic field dependence of the oscillations in $\nu = 1$ demonstrating Aharonov-Bohm periodicity; the magnetic field period yields $\phi_0/\Delta B_1 = 0.80\ \mu\text{m}^2$, consistent with a small reduction of the area enclosed by the edge state within the designed area of 1.1 μm^2. (**C**) 100 repeated V_{PG} sweeps in $\nu = 1/3$, using the same sweeping parameters as in (A), demonstrating the stochastic fluctuations induced by the RTN that could easily be mistaken for structure-less noise, especially if averaged over by a slow sweep. (**D**) 6 of the V_{PG} sweeps plotted to demonstrate switching between the three sinusoidal branches within a single scan. (**E**) 2D histograms showing the probability of measuring a given conductance for each V_{PG} value and its trend with the magnetic field. All three branches (partially highlighted) are made evident by this plot, and each branch trends identically with a flux super-period in the magnetic field corresponding to $e/3$ anyons. Note that (E) is effectively presenting the AB oscillation demonstrated in the B versus V_{PG} plane for the $\nu = 1/3$ case, where RTN is present during each scan of V_{PG}.

field period for a single branch to return to its initial V_{PG} coordinate) yields $3\phi_0/\Delta B_{1/3} = 0.83 \pm 0.04\ \mu\text{m}^2$. This value is what one expects for interfering $e/3$ quasiparticles such that $\phi_0 \to h/(e/3) = 3\phi_0$. We similarly observe AB interference and a flux super-periodicity on the fractional edge of $\nu = 4/3$ (Fig. S4), whereas the integer edge shows typical electron AB interference with no observable RTN. Note that even if the charge within the interferometer fluctuates in the integer case, the change in the interference phase caused by integer changes in electron charge will be a multiple of 2π and therefore unobservable [40].

The fact that all tested configurations show AB interference (i.e. a negative slope of constant phase with respect to V_{PG} and B) instead of Coulomb-dominated effects indicates that our graphene interferometer is sufficiently screened by the graphite gates to suppress long-range Coulomb interaction, as required for observing braiding signatures [7, 14, 17]. Furthermore, the observed $3\phi_0$ magnetic-flux super-period in both $\nu = 1/3$ and $\nu = 4/3$ agrees with the $3\phi_0$ super-period observed near the center of the $\nu = 1/3$ plateau in GaAs-based FP interferometers [7, 17], suggesting that the quasiparticle gap is large enough to prevent continuous addition of quasiparticles [52].

The repeated sweep method exhibited in Fig. 2, which includes hundreds of phase jumps, provides an opportune data set to extract a precise value for the anyon

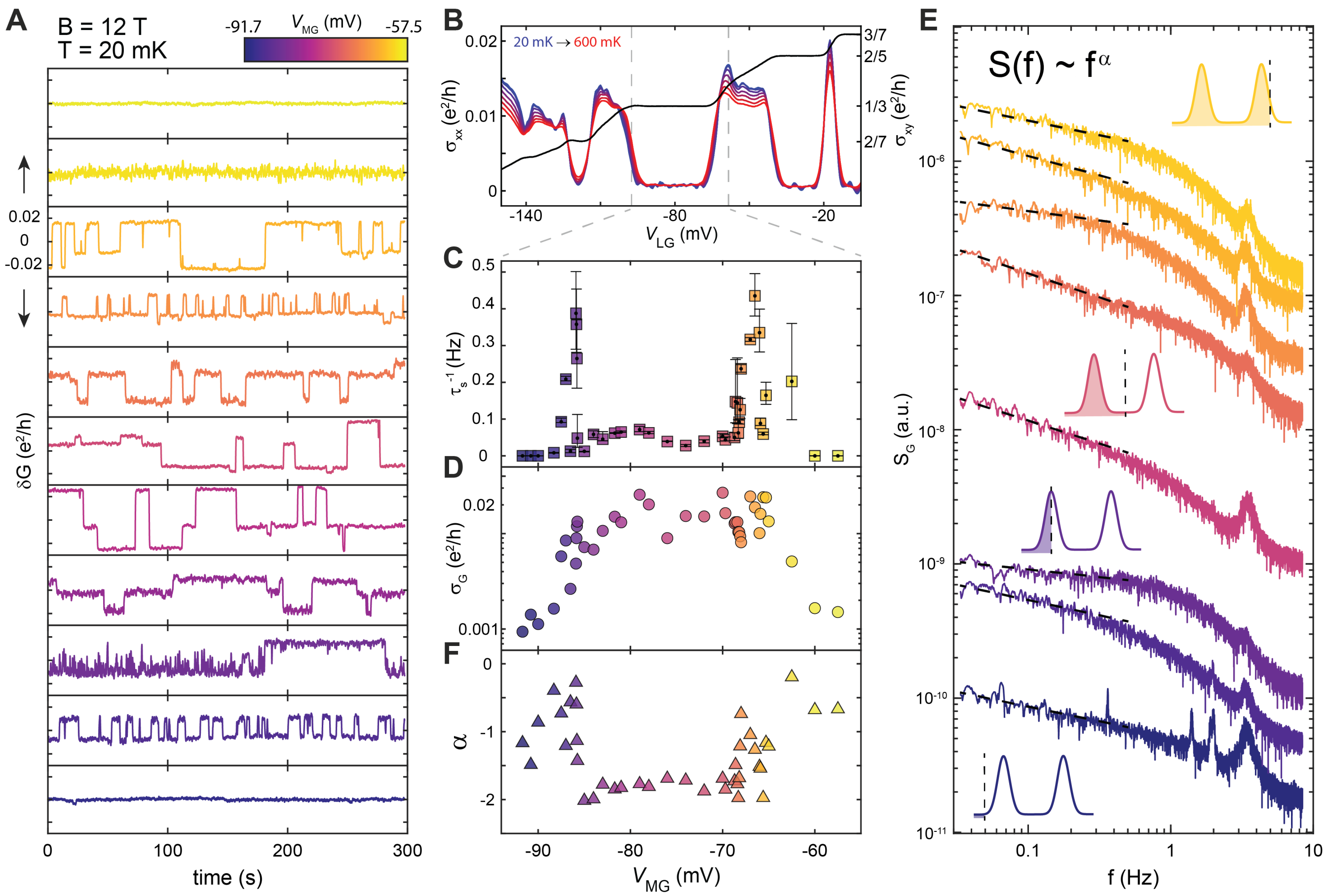

FIG. 3. **Telegraph noise dependence on filling in $\nu = 1/3$.** (**A**) Conductances versus time taken at different values for V_{MG}, indicated by color bar. The 300 seconds shown are from longer 50 minute datasets. (**B**) Hall data taken from the left half of the device with density tuned via V_{LG}. The dashed lines indicate the associated range shown for V_{MG} in (C-E) below. The color scale on σ_{xx} spans from 20 mK (blue) to 600 mK (red). (**C**) Average branch switching rate along the plateau. Error bars indicate uncertainty associated with the switching identification algorithm and background noise (see section 2 of [49]). (**D**) Standard deviation of conductance computed for $G(t)$ at fixed V_{MG}. (**E**) The spectral densities of conductance plotted on a log-log scale (traces are arbitrarily vertically shifted by ordering of V_{MG}). Dotted lines are fit to the power law dependence f^{α} in the low frequency regime. Inset cartoons indicate the anyonic quasiparticle density of states versus energy, with the vertical dashed lines indicating the Fermi level for a given filling. (**F**) The exponent α extracted from the fits of the power spectrum in (E) within the frequency range associated with the RTN.

braiding phase and associated uncertainty (see Section 3 of [49] for methodology and detailed discussion). For the subplots shown in Fig. 2E, each containing 100 repeated sweeps and several hundred branch switches, we extract an average braiding phase of $2\pi(0.3336 \pm 0.0051)$, or $120.1° \pm 1.8°$. The phase shift closely agrees with the theoretical value $2\pi/3$ and with the value extracted from previous interferometer [7, 17] and anyon collider [6] experiments. Additionally, the smallness of the fitting error to the theoretical value $2\pi/3$, which neglects Coulomb corrections to the interferometer area with each quasiparticle fluctuation, demonstrates that Coulomb corrections are indeed negligible in our device.

Telegraph noise across the quantum Hall plateau

We gain insight into the nature of the quasiparticle fluctuations by tracking how the RTN evolves with density (filling) across the FQH plateau. Figure 3A exhibits subsets of 50 minute measurements of the conductance, showing the V_{MG} dependent RTN across the $\nu = 1/3$ plateau. The trace colors indicate the select values of V_{MG} that correspond to the subrange of the $\nu = 1/3$ QH plateau as shown in Fig. 3B. Of immediate note are clear changes in both the switching rate and amplitude as V_{MG} steps across the plateau. The average switching rate from the complete 50 minute traces, τ_s^{-1}, shown in Fig. 3C, exhibits steep rises near the edges of the plateau and a relatively constant switching rate in between. Figure 3D shows the standard deviation, σ_G, of the diagonal con-

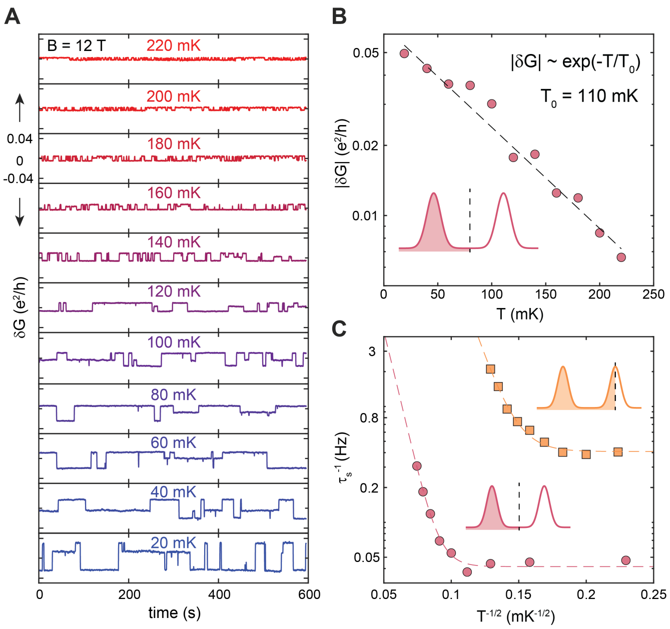

FIG. 4. **Temperature dependent telegraph noise and visibility in $\nu = 1/3$.** (**A**) Conductance versus time taken at different temperatures T. The 600 seconds shown are subsets of longer 50 minute datasets used for subsequent analysis. (**B**) Oscillation visibility extracted from V_{PG} sweep measurements (21 repeated scans averaged per point). The exponential decay fit to the oscillation visibility results in a characteristic temperature $T_0 = 110$ mK. (**C**) Low-temperature saturation and high-temperature activation of the average switching rate τ_s^{-1} observed for two fillings: at the center and at the edge of the $\nu = 1/3$ plateau, as shown in the insets. Shown fit lines follow the empirical formula of Eq. 2., where $T_{ES} = 22$ K (middle of plateau) and $T_{ES} = 9.5$ K (edge of plateau), which correspond to VRH hopping lengths of 130 nm and 300 nm, respectively [50, 51]

ductance $G(t)$, providing a direct measure of switching amplitude.

The striking behavior of the anyon branch switching rate and amplitude along the plateau reveals that the quasiparticle fluctuations and coherence are closely correlated with the compressibility of the FQH state. A natural explanation would be that the switching rate increases as the number of localized states and anyon trapping sites increases near the edges of the FQH plateau. However, a simple increase in the individual switching rates of a constant number of traps across the plateau cannot be ruled out from this observation alone.

The noise spectral density of the diagonal conductance, S_G, can provide additional information supporting the hypothesis of an increasing trap number near the edge of the plateau. Figure 3E shows S_G as a function of frequency f, obtained from the Fourier transform of $G(t)$ at various V_{MG} values across the plateau region. We find that $S_G(f)$ follows a power law scaling behavior $\sim f^{\alpha}$ in the low frequency regime corresponding to the RTN signal. Figure 3F exhibits the scaling exponent α obtained from the line fits shown in Fig. 3E. In the middle of the plateau, the exponent α remains close to -2, which is expected from RTN with a single switching timescale [53]. However, near the edges α sharply increases and deviates from this stable value. It is known that when many instances of RTN with different switching timescales are convolved together, S_G is expected to approach $1/f$, or $\alpha = -1$ [54]. Accordingly, the change of α near the edges of the plateau suggests that there are more unique switching timescales at the edge of the plateau than in the middle. This observation, together with the switching rate behavior discussed above, supports that the increased branch switching incidents are indeed associated with increased localized anyon states in the bulk.

Temperature scaling

We also study how the RTN changes as a function of temperature T. Figure 4A shows $G(t)$ near the middle of the $\nu = 1/3$ plateau at T ranging from 20 mK to 220 mK. As temperature increases, the switching amplitude decreases corresponding to a decrease in AB oscillation visibility. Figure 4B shows separately measured AB oscillation visibility as a function of T using plunger gate sweep measurements (similar to Fig. 2,C-E). The visibility decreases following an exponential decay as T increases, with a characteristic energy scale $T_0 = 110$ mK similar to that observed in $\nu = 1/3$ in GaAs [7].

In addition to the decrease in visibility, the RTN also shows an increase in switching rate as temperature increases. Figure 4C shows temperature dependent τ_s^{-1} for two representative data sets, one at the center (red) and the other at the edge (yellow) of the plateau. While the switching rate increases quickly at the high temperature limit, there is a dramatic flat saturation of τ_s^{-1} for both data sets at low temperatures, below about 100 mK and 50 mK for the plateau center and edge, respectively. We find that an empirical formula which combines a term motivated by an Efros-Shlovskii (ES) form of variable-range hopping (VRH) [55, 56] with an additional temperature-independent transition rate, $\tau_{s,0}^{-1}$,

$$\tau_s^{-1} = \tau_{s,0}^{-1} + \tau_{s,1}^{-1}(T)\ e^{-(T_{ES}/T)^{1/2}} \tag{2}$$

can provide a reasonable fit to the data as shown by the dashed lines in Fig. 4C. Here $\tau_{s,1}^{-1}(T) \sim 1/T$ and T_{ES} is the characteristic ES VRH temperature scale. Although VRH has been used in the past to model longitudinal conduction caused by localized states in the quantum Hall effect [50, 56–58], the physical mechanism behind the temperature scaling of τ_s^{-1} here remains nebulous.

Although we were able to provide evidence that the anyon fluctuations are closely associated with the number of anyon localized states, and that they have consistent temperature scaling properties, a precise mechanism for their origin remains unclear. Based on the uniformity of the AB-modulating sinusoids in Figs. 1F and 2E, we postulate that the anyons are neither hopping from nor getting trapped within regions close to the QPCs, as even small changes in environmental charge would drastically change their tunings and the resultant visibility of the interference signal over time. We also observe that enclosing the sample in an additional radiation shield strongly reduces the switching rate (Fig. S9), indicating that photons stimulate the fluctuations. Lastly, although fluctuations have not been reported in GaAs heterostructure-based interferometry experiments [7, 17, 44, 59, 60] and more recently in bilayer graphene [61], we note that the presence of slower or faster switching timescales could make initial observations of anyon fluctuations challenging with standard DC measurement techniques.

Discussion and Outlook

In this work, we have shown that anyonic quasiparticle fluctuations and the resulting RTN in a FP interferometer can be used as a powerful tool to exhibit the complete set of braiding phases present in abelian states. These techniques pave the way for future interferometer measurements of non-abelian anyon braiding in even-denominator FQH states, where the small energy gap may enhance the RTN and limit the range of AB phase modulation. Several theoretical studies have already discussed which signatures would be expected in such a case where RTN is present for non-abelian states [41–43]. Moreover, our ability to observe the slow equilibration of anyons enables future experiments to probe nontrivial anyon dynamics and to dynamically control anyon number in similar devices. This is particularly relevant to the ultimate goal of constructing a topological qubit with non-abelian anyons, which requires an understanding of how to selectively control and modulate the quasiparticle number [62–64].

Note added: During the preparation of this manuscript, we became aware of a concurrent work using a similar graphene device [65].

[1] R. B. Laughlin, Anomalous Quantum Hall Effect: An Incompressible Quantum Fluid with Fractionally Charged Excitations, Physical Review Letters **50**, 1395 (1983).

[2] B. I. Halperin, Statistics of Quasiparticles and the Hierarchy of Fractional Quantized Hall States, Physical Review Letters **52**, 1583 (1984).

[3] D. Arovas, J. R. Schrieffer, and F. Wilczek, Fractional Statistics and the Quantum Hall Effect, Physical Review Letters **53**, 722 (1984).

[4] A. Stern, Anyons and the quantum Hall effect—A pedagogical review, Annals of Physics **323**, 204 (2008).

[5] D. E. Feldman and B. I. Halperin, Fractional charge and fractional statistics in the quantum Hall effects, Reports on Progress in Physics **84**, 076501 (2021).

[6] H. Bartolomei, M. Kumar, R. Bisognin, A. Marguerite, J.-M. Berroir, E. Bocquillon, B. Plaçais, A. Cavanna, Q. Dong, U. Gennser, Y. Jin, and G. Fève, Fractional statistics in anyon collisions, Science **368**, 173 (2020).

[7] J. Nakamura, S. Liang, G. C. Gardner, and M. J. Manfra, Direct observation of anyonic braiding statistics, Nature Physics **16**, 931 (2020).

[8] A. Kitaev, Anyons in an exactly solved model and beyond, Annals of Physics January Special Issue, **321**, 2 (2006).

[9] C. Nayak, S. H. Simon, A. Stern, M. Freedman, and S. Das Sarma, Non-Abelian anyons and topological quantum computation, Reviews of Modern Physics **80**, 1083 (2008).

[10] A. Stern and N. H. Lindner, Topological Quantum Computation—From Basic Concepts to First Experiments, Science **339**, 1179 (2013).

[11] S. D. Sarma, M. Freedman, and C. Nayak, Majorana zero modes and topological quantum computation, npj Quantum Information **1**, 1 (2015).

[12] A. Yazdani, F. von Oppen, B. I. Halperin, and A. Yacoby, Hunting for Majoranas, Science **380**, eade0850 (2023).

[13] C. de C. Chamon, D. E. Freed, S. A. Kivelson, S. L. Sondhi, and X. G. Wen, Two point-contact interferometer for quantum Hall systems, Physical Review B **55**, 2331 (1997).

[14] B. I. Halperin, A. Stern, I. Neder, and B. Rosenow, Theory of the fabry-pérot quantum hall interferometer, Physical Review B **83**, 155440 (2011).

[15] M. Carrega, L. Chirolli, S. Heun, and L. Sorba, Anyons in quantum Hall interferometry, Nature Reviews Physics **3**, 698 (2021).

[16] N. Read and S. Das Sarma, Clarification of braiding statistics in Fabry–Perot interferometry, Nature Physics **20**, 381 (2024).

[17] J. Nakamura, S. Liang, G. C. Gardner, and M. J. Manfra, Impact of bulk-edge coupling on observation of anyonic braiding statistics in quantum Hall interferometers, Nature Communications **13**, 344 (2022).

[18] J. Nakamura, S. Fallahi, H. Sahasrabudhe, R. Rahman, S. Liang, G. C. Gardner, and M. J. Manfra, Aharonov–Bohm interference of fractional quantum Hall edge modes, Nature Physics **15**, 563 (2019).

[19] K. Zimmermann, A. Jordan, F. Gay, K. Watanabe, T. Taniguchi, Z. Han, V. Bouchiat, H. Sellier, and B. Sacépé, Tunable transmission of quantum Hall edge channels with full degeneracy lifting in split-gated graphene devices, Nature Communications **8**, 14983 (2017).

[20] H. Overweg, H. Eggimann, X. Chen, S. Slizovskiy, M. Eich, R. Pisoni, Y. Lee, P. Rickhaus, K. Watanabe, T. Taniguchi, V. Fal'ko, T. Ihn, and K. Ensslin, Electro-

statically Induced Quantum Point Contacts in Bilayer Graphene, Nano Letters **18**, 553 (2018).
[21] C. Déprez, L. Veyrat, H. Vignaud, G. Nayak, K. Watanabe, T. Taniguchi, F. Gay, H. Sellier, and B. Sacépé, A tunable Fabry–Pérot quantum Hall interferometer in graphene, Nature Nanotechnology **16**, 555 (2021).
[22] Y. Ronen, T. Werkmeister, D. Haie Najafabadi, A. T. Pierce, L. E. Anderson, Y. J. Shin, S. Y. Lee, Y. H. Lee, B. Johnson, K. Watanabe, T. Taniguchi, A. Yacoby, and P. Kim, Aharonov–Bohm effect in graphene-based Fabry–Pérot quantum Hall interferometers, Nature Nanotechnology **16**, 563 (2021).
[23] L. Zhao, E. G. Arnault, T. F. Q. Larson, Z. Iftikhar, A. Seredinski, T. Fleming, K. Watanabe, T. Taniguchi, F. Amet, and G. Finkelstein, Graphene-Based Quantum Hall Interferometer with Self-Aligned Side Gates, Nano Letters **22**, 9645 (2022).
[24] H. Fu, K. Huang, K. Watanabe, T. Taniguchi, M. Kayyalha, and J. Zhu, Aharonov–Bohm Oscillations in Bilayer Graphene Quantum Hall Edge State Fabry–Pérot Interferometers, Nano Letters **23**, 718 (2023).
[25] T. Werkmeister, J. R. Ehrets, Y. Ronen, M. E. Wesson, D. Najafabadi, Z. Wei, K. Watanabe, T. Taniguchi, D. E. Feldman, B. I. Halperin, A. Yacoby, and P. Kim, Strongly coupled edge states in a graphene quantum Hall interferometer, Nature Communications **15**, 6533 (2024).
[26] W. Yang, D. Perconte, C. Déprez, K. Watanabe, T. Taniguchi, S. Dumont, E. Wagner, F. Gay, I. Safi, H. Sellier, and B. Sacépé, Evidence for correlated electron pairs and triplets in quantum Hall interferometers, Nature Communications **15**, 10064 (2024).
[27] Y. Zeng, J. I. A. Li, S. A. Dietrich, O. M. Ghosh, K. Watanabe, T. Taniguchi, J. Hone, and C. R. Dean, High-Quality Magnetotransport in Graphene Using the Edge-Free Corbino Geometry, Physical Review Letters **122**, 137701 (2019).
[28] R. Ribeiro-Palau, S. Chen, Y. Zeng, K. Watanabe, T. Taniguchi, J. Hone, and C. R. Dean, High-Quality Electrostatically Defined Hall Bars in Monolayer Graphene, Nano Letters **19**, 2583 (2019).
[29] L. A. Cohen, N. L. Samuelson, T. Wang, K. Klocke, C. C. Reeves, T. Taniguchi, K. Watanabe, S. Vijay, M. P. Zaletel, and A. F. Young, Nanoscale electrostatic control in ultraclean van der Waals heterostructures by local anodic oxidation of graphite gates, Nature Physics , 1 (2023).
[30] L. A. Cohen, N. L. Samuelson, T. Wang, T. Taniguchi, K. Watanabe, M. P. Zaletel, and A. F. Young, Universal chiral Luttinger liquid behavior in a graphene fractional quantum Hall point contact, Science **382**, 542 (2023).
[31] A. A. Zibrov, C. Kometter, H. Zhou, E. M. Spanton, T. Taniguchi, K. Watanabe, M. P. Zaletel, and A. F. Young, Tunable interacting composite fermion phases in a half-filled bilayer-graphene Landau level, Nature **549**, 360 (2017).
[32] J. I. A. Li, C. Tan, S. Chen, Y. Zeng, T. Taniguchi, K. Watanabe, J. Hone, and C. R. Dean, Even-denominator fractional quantum Hall states in bilayer graphene, Science **358**, 648 (2017).
[33] K. Huang, H. Fu, D. R. Hickey, N. Alem, X. Lin, K. Watanabe, T. Taniguchi, and J. Zhu, Valley Isospin Controlled Fractional Quantum Hall States in Bilayer Graphene, Physical Review X **12**, 031019 (2022).
[34] A. Assouline, T. Wang, H. Zhou, L. A. Cohen, F. Yang, R. Zhang, T. Taniguchi, K. Watanabe, R. S. K. Mong, M. P. Zaletel, and A. F. Young, Energy Gap of the Even-Denominator Fractional Quantum Hall State in Bilayer Graphene, Physical Review Letters **132**, 046603 (2024).
[35] Y. Hu, Y.-C. Tsui, M. He, U. Kamber, T. Wang, A. S. Mohammadi, K. Watanabe, T. Taniguchi, Z. Papic, M. P. Zaletel, and A. Yazdani, High-Resolution Tunneling Spectroscopy of Fractional Quantum Hall States (2023), arxiv:2308.05789 [cond-mat].
[36] C. R. Dean, A. F. Young, I. Meric, C. Lee, L. Wang, S. Sorgenfrei, K. Watanabe, T. Taniguchi, P. Kim, K. L. Shepard, and J. Hone, Boron nitride substrates for high-quality graphene electronics, Nature Nanotechnology **5**, 722 (2010).
[37] S. Baer, C. Rössler, E. C. de Wiljes, P.-L. Ardelt, T. Ihn, K. Ensslin, C. Reichl, and W. Wegscheider, Interplay of fractional quantum Hall states and localization in quantum point contacts, Physical Review B **89**, 085424 (2014).
[38] N. Ofek, A. Bid, M. Heiblum, A. Stern, V. Umansky, and D. Mahalu, Role of interactions in an electronic Fabry–Perot interferometer operating in the quantum Hall effect regime, Proceedings of the National Academy of Sciences **107**, 5276 (2010).
[39] D. T. McClure, W. Chang, C. M. Marcus, L. N. Pfeiffer, and K. W. West, Fabry-Perot Interferometry with Fractional Charges, Physical Review Letters **108**, 256804 (2012).
[40] D. E. Feldman and B. I. Halperin, Robustness of quantum Hall interferometry, Physical Review B **105**, 165310 (2022).
[41] C. L. Kane, Telegraph Noise and Fractional Statistics in the Quantum Hall Effect, Physical Review Letters **90**, 226802 (2003).
[42] E. Grosfeld, S. H. Simon, and A. Stern, Switching Noise as a Probe of Statistics in the Fractional Quantum Hall Effect, Physical Review Letters **96**, 226803 (2006).
[43] B. Rosenow and S. H. Simon, Telegraph noise and the Fabry-Perot quantum Hall interferometer, Physical Review B **85**, 201302 (2012).
[44] J. Nakamura, S. Liang, G. C. Gardner, and M. J. Manfra, Fabry-Pérot Interferometry at the $\nu = 2\ /\ 5$ Fractional Quantum Hall State, Physical Review X **13**, 041012 (2023).
[45] Y. Zhang, D. T. McClure, E. M. Levenson-Falk, C. M. Marcus, L. N. Pfeiffer, and K. W. West, Distinct signatures for Coulomb blockade and Aharonov-Bohm interference in electronic Fabry-Perot interferometers, Physical Review B **79**, 241304 (2009).
[46] C. W. von Keyserlingk, S. H. Simon, and B. Rosenow, Enhanced Bulk-Edge Coulomb Coupling in Fractional Fabry-Perot Interferometers, Physical Review Letters **115**, 126807 (2015).
[47] M. P. Röösli, L. Brem, B. Kratochwil, G. Nicolí, B. A. Braem, S. Hennel, P. Märki, M. Berl, C. Reichl, W. Wegscheider, K. Ensslin, T. Ihn, and B. Rosenow, Observation of quantum Hall interferometer phase jumps due to a change in the number of bulk quasiparticles, Physical Review B **101**, 125302 (2020).
[48] M. P. Röösli, M. Hug, G. Nicolí, P. Märki, C. Reichl, B. Rosenow, W. Wegscheider, K. Ensslin, and T. Ihn, Fractional Coulomb blockade for quasi-particle tunneling between edge channels, Science Advances **7**, eabf5547 (2021).
[49] See supplementary materials.

[50] K. Bennaceur, P. Jacques, F. Portier, P. Roche, and D. C. Glattli, Unveiling quantum Hall transport by Efros-Shklovskii to Mott variable-range hopping transition in graphene, Physical Review B **86**, 085433 (2012).

[51] A. L. Efros, N. Van Lien, and B. I. Shklovskii, Variable range hopping in doped crystalline semiconductors, Solid State Communications **32**, 851 (1979).

[52] B. Rosenow and A. Stern, Flux Superperiods and Periodicity Transitions in Quantum Hall Interferometers, Physical Review Letters **124**, 106805 (2020).

[53] M. B. Weissman, 1/f noise and other slow, nonexponential kinetics in condensed matter, Reviews of Modern Physics **60**, 537 (1988).

[54] Sh. Kogan, 1/f noise and random telegraph noise, in *Electronic Noise and Fluctuations in Solids* (Cambridge University Press, Cambridge, 1996) pp. 203–286.

[55] A. L. Efros and B. I. Shklovskii, Coulomb gap and low temperature conductivity of disordered systems, Journal of Physics C: Solid State Physics **8**, L49 (1975).

[56] G. Ebert, K. von Klitzing, C. Probst, E. Schuberth, K. Ploog, and G. Weimann, Hopping conduction in the Landau level tails in GaAs-AlxGa1-xAs heterostructures at low temperatures, Solid State Communications **45**, 625 (1983).

[57] A. J. M. Giesbers, U. Zeitler, L. A. Ponomarenko, R. Yang, K. S. Novoselov, A. K. Geim, and J. C. Maan, Scaling of the quantum Hall plateau-plateau transition in graphene, Physical Review B **80**, 241411 (2009).

[58] J. Martin, S. Ilani, B. Verdene, J. Smet, V. Umansky, D. Mahalu, D. Schuh, G. Abstreiter, and A. Yacoby, Localization of Fractionally Charged Quasi-Particles, Science **305**, 980 (2004).

[59] R. L. Willett, K. Shtengel, C. Nayak, L. N. Pfeiffer, Y. J. Chung, M. L. Peabody, K. W. Baldwin, and K. W. West, Interference measurements of non-abelian $e/4$ & abelian $e/2$ quasiparticle braiding, Physical Review X **13**, 011028 (2023).

[60] H. K. Kundu, S. Biswas, N. Ofek, V. Umansky, and M. Heiblum, Anyonic interference and braiding phase in a Mach-Zehnder interferometer, Nature Physics **19**, 515 (2023).

[61] J. Kim, H. Dev, R. Kumar, A. Ilin, A. Haug, V. Bhardwaj, C. Hong, K. Watanabe, T. Taniguchi, A. Stern, and Y. Ronen, Aharonov-Bohm interference and the evolution of phase jumps in fractional quantum Hall Fabry-Perot interferometers based on bi-layer graphene, Nature Nanotechnology **19**, 1619 (2024).

[62] S. Das Sarma, M. Freedman, and C. Nayak, Topologically Protected Qubits from a Possible Non-Abelian Fractional Quantum Hall State, Physical Review Letters **94**, 166802 (2005).

[63] A. Stern and B. I. Halperin, Proposed experiments to probe the non-abelian $\nu = 5/2$ quantum hall state, Physical Review Letters **96**, 016802 (2006).

[64] P. Bonderson, A. Kitaev, and K. Shtengel, Detecting Non-Abelian Statistics in the $\nu = 5\ /\ 2$ Fractional Quantum Hall State, Physical Review Letters **96**, 016803 (2006).

[65] N. L. Samuelson, L. A. Cohen, W. Wang, S. Blanch, T. Taniguchi, K. Watanabe, M. P. Zaletel, and A. F. Young, Anyonic statistics and slow quasiparticle dynamics in a graphene fractional quantum Hall interferometer (2024), arxiv:2403.19628 [cond-mat].

[66] T. Werkmeister and J. Ehrets, Data for "Anyon braiding and telegraph noise in a graphene interferometer", https://doi.org/10.5281/zenodo.14947934 (2025).

Acknowledgments

We thank Abhishek Banerjee, Nick Poniatowski, Yuval Ronen, Steven H. Simon, and Jonathan Zauberman for stimulating and helpful discussions. **Funding:** The major part of the experiment was supported by DOE (DE-SC0012260). J.R.E. acknowledges support from ARO MURI (N00014-21-1-2537) for sample preparation, measurement, characterization, and analysis. K.W. and T.T. acknowledge support from the JSPS KAKENHI (Grant Numbers 20H00354 and 23H02052) and World Premier International Research Center Initiative (WPI), MEXT, Japan. M.E.W. and A.Y. acknowledge support from Quantum Science Center (QSC), a National Quantum Information Science Research Center of the U.S. Department of Energy (DOE). B.I.H. acknowledges support from NSF grant DMR-1231319. Nanofabrication was performed at the Center for Nanoscale Systems at Harvard, supported in part by an NSF NNIN award ECS-00335765. **Author contributions:** T.W., J.R.E., and P.K. conceived of and designed the experiment. T.W. and D.H.N. created the van der Waals heterostructure. T.W. performed the nanofabrication. T.W. and J.R.E. performed the measurements. M.E.W. and A.Y. provided the measurement cryostat and collaborated on discussions and analysis. K.W. and T.T. provided the hexagonal boron nitride crystals. T.W., J.R.E., and P.K. analyzed the data and wrote the manuscript with contributions from B.I.H. **Competing interests:** The authors declare no competing interests. **Data and materials availability:** All gathered data and code used to generate the plots within this paper are available at a repository hosted on Zenodo [66].

SUPPLEMENTARY MATERIALS

Materials and methods
Supplementary text
Figures S1-S9